Journal of Cluster Science (2023) 34:211–222
https://doi.org/10.1007/s10876-021-02217-y

ORIGINAL PAPER

Increased Pro-Apoptotic and Anti-Proliferative Activities of Simvastatin Encapsulated PCL-PEG Nanoparticles on Human Breast Cancer Adenocarcinoma Cells

Mehdi Dadashpour[1,2] · Meysam Ganjibakhsh[3] · Hanieh Mousazadeh[4] · Kazem Nejati[5]

Received: 5 September 2021 / Accepted: 19 December 2021 / Published online: 6 January 2022

Abstract

Recently, Simvastatin (SIM) is received notable attention due to its anti-cancer properties. However, the lipophilicity feature of SIM restricted its application as a chemotherapy agent. This work aimed to investigate the Polycaprolactone–Polyethylene Glycol (PCL-PEG) efficiency as the nano-carrier for SIM to enhance its anti-cancer properties. Dynamic Light Scattering (DLS), field emission scanning electron microscopy (FE-SEM), and Fourier transform infrared (FTIR) were used to characterize drug-loaded nanoparticles (NPs). To study apoptotic and anti-proliferative properties of drug-loaded NPs, flow cytometry and MTT assays were utilized. The real-time PCR method measured the expression of apoptotic genes Bcl-2, Bax, Fas and cell cycle regulating genes, p53, cyclin D, and Rb. MTT assay indicated that loading SIM on PCL-PEG NPs increased cytotoxicity dose-dependently. In addition, a noticeable increase was found in the sub-G1 population of treated cells with drug-loaded NPs than free SIM. The remarkable up-regulation of Bax, Fas and p53 genes was detected in treated MCF-7 cells with the decrease of Bcl2, Rb, and Cyclin D 1 gene expression in cells treated with drug-loaded NPs than free SIM. Taken together, these results show that the polymeric PCL-PEG NPs systems represent a promising new therapeutic approach for the treatment of breast cancer.

Keywords Simvastatin · Polymeric nanoparticles · Anticancer · Apoptosis · Breast cancer

Introduction

Breast cancer is one of the most prevalent invasive cancer in adult women. Chemotherapy, radiation, and surgery are the most famous treatments for breast cancer. However, radiation therapy and chemotherapy have some limitations due to unpleasant side effects [1]. Although chemotherapy is a suitable approach, breast cancer cells have recently been indicated to be resistant to various chemotherapeutics [2]. The standard gold treatment for breast cancer was surgery supported by adjuvant therapy for a long time. In recent years, neoadjuvant treatment has been the main approach in cancer therapy [3]. The motility and metastases of breast cancer cells generally happen because of Rho proteins overexpression as major regulators of the cytoskeleton and actin-dependent processes, including cell polarity and migration in addition to cell-cycle progression and gene expression [4].

Currently, various non-hazardous bioactive ingredients like statins and their ability to reduce cancer relapse and

✉ Kazem Nejati
k.nejati@arums.ac.ir

1 Department of Medical Biotechnology, Semnan University of Medical Sciences, Semnan, Iran

2 Biotechnology Research Center, Semnan University of Medical Sciences, Semnan, Iran

3 Advanced Therapy Medicinal Product Technology Development Center, Royan Institute for Stem Cell Biology and Technology, Academic Center for Education, Culture and Research, Tehran, Iran

4 Department of Clinical Biochemistry and Laboratory Medicine, Faculty of Medicine, Tabriz University of Medical Sciences, Tabriz, Iran

5 Pharmaceutical Sciences Research Center, Ardabil University of Medical Sciences, Ardabil, Iran

improve treatment have been evaluated [5–7]. Statins, as inhibitors of the mevalonate pathway, decrease the synthesis of geranylgeranyl pyrophosphate (GGPP) and farnesyl pyrophosphate (FPP), the two key isoprenoid metabolites in the mevalonate pathway [8]. Blocking the prenylation of Rho proteins through inhibition of GGPP and FPP production and decreasing their synthesis is regarded as an effective chemoprevention strategy for statins [9]. Accordingly, the use of statins is increasing due to their potential anti-cancer activity and chemotherapeutic effects. Statins, in particular, can permeate cell membranes and directly affect cell functions in tumor cells [10].

SIM, a lipid-lowering drug, is an inhibitor of 3-hydroxy-3-methyl glutaryl-coenzyme A (HMG-CoA) reductase that blocks mevalonic acid biosynthesis which is a cholesterol precursor [11]. It is confirmed that malignant breast cancer cells possess a raised level of mevalonate [12]. Probably high level of mevalonate synthesis in cancer cells occurs due to increased requirements for a mevalonate-derived metabolite in response to the rapid proliferation of tumor cells. Hence, it is shown that SIM causes arrest of the cell cycle in cancerous breast cells and even in cancerous stem cells, which leads to triggering apoptosis [12].

Short half-life, low solubility, poor biological availability, low duration of stability in the bloodstream, and rapid metabolism and degradation are the main limitations of using pharmaceutical compounds such as SIM in medicine. A potential alternative strategy for overcoming these drawbacks and enhancing its anti-cancer activity is using a nanotechnology-based strategy that may improve the chemo-preventive and chemotherapeutic effects [13].

Polymeric particles are a distinctive type of nanomaterials that have found many new applications in delivery systems for in situ controlled release of therapeutic applications [14, 15]. Nanoparticle drug delivery supplies numerous advantages due to high encapsulation efficiency, a protected drug from degradation, improved bio-distribution, delivered, and controlled drug release [16–18]. One of the most successful polymer nanoparticles is Polycaprolactone–Polyethylene Glycol (PCL-PEG). PEG is a useful hydrophilic polymer for avoiding phagocytosis of reticuloendothelial system (RES) and prolong their cycling time in vivo and PCL is a hydrophobic polymer that can be couple with PEG to form amphiphilic copolymer [19, 20].These copolymers are biocompatible and biodegradable materials that have shown high potential in drug-delivery systems [21]. They are non-toxic, non-immunogenic and also their degradation products can enter the Krebs cycle or excrete by the urinary system. Moreover, PCL-PEG copolymers have a high drug-loading capacity, high potential to enhance drug solubility, sustained-release properties, prolonged systemic circulation time, the ability to escape recognition by macrophages, and show high potential to be a success in the development of new systems for drug delivery [22]. Hence, encapsulating anti-cancer phytochemicals such as SIM in PCL/PEG biodegradable nanoparticles may have many advantages over other drug delivery systems.

In the current study, we aimed to encapsulate SIM compound into PCL/PEG (nanoparticles) NPs and investigate its pro-apoptotic and anti-cancer activities on MCF-7 human breast cancer adenocarcinoma cells through modulating the expression of apoptotic and cell cycle genes, as the important molecules involved in tumorigenesis.

Materials and Methods

Chemicals and Materials

Polyvinyl alcohol, dichloromethane, dimethyl sulfoxide, stannous octoate, glycolide, DL-Lactide, PEG (MW2000) were obtained from Sigma-Aldrich (Saint Quentin Fallavier, France) Roswell Park Memorial Institute (RPMI) 1640, fetal bovine serum (FBS), 3(4, 5-dimethylthiazol-2-yl) 2, 5-diphenyltetrazolium bromide (MTT), 4', 6-diamidino-2-phenylindole (DAPI), tetrazolium salt and propidium iodide (PI) were purchased from Santa Cruz Biotechnology (Santa Cruz, CA, USA) Annexin V/PI was obtained from eBioscience (San Diego, CA, USA).

Preparation of Copolymer

The copolymers were synthesized according to our previous report. It was synthesized by a ring opening polymerization of ε-caprolactone with PEG as initial molecule and Sn $(Oct)_2$ as catalyst. In brief, PEG (2 g) was added to a dry three necked flask and heated at 120 °C under vacuum for 3 h (h) to remove moisture. The ε-caprolactone (4 g) and Sn(Oct)2 (0.01 mmol) were introduced into the flask under a nitrogen atmosphere and then the polymerization reaction was performed at 120 °C with vigorous stirring for 12 h. After 12 h, the resulting copolymer was cooled at room temperature, dissolved in chloroform and precipitated in cold diethyl ether. The copolymer was dried under vacuum at room temperature for 24 h.

Preparation of Drug-Loaded NPs

SIM loaded polymers were prepared by a double emulsion technique (w/o/w). 1 mL aqueous solution of SIM with known concentration 6 mg/mL was first poured dropwise into the PCL- PEG copolymer solution in 2 mL chloroform (25 mg/mL) under certain mixing rates (1500 rpm) to form a w/o emulsion. The resulting emulsion was then injected drop-wise into 20 mL of distillated water containing 0.4 wt

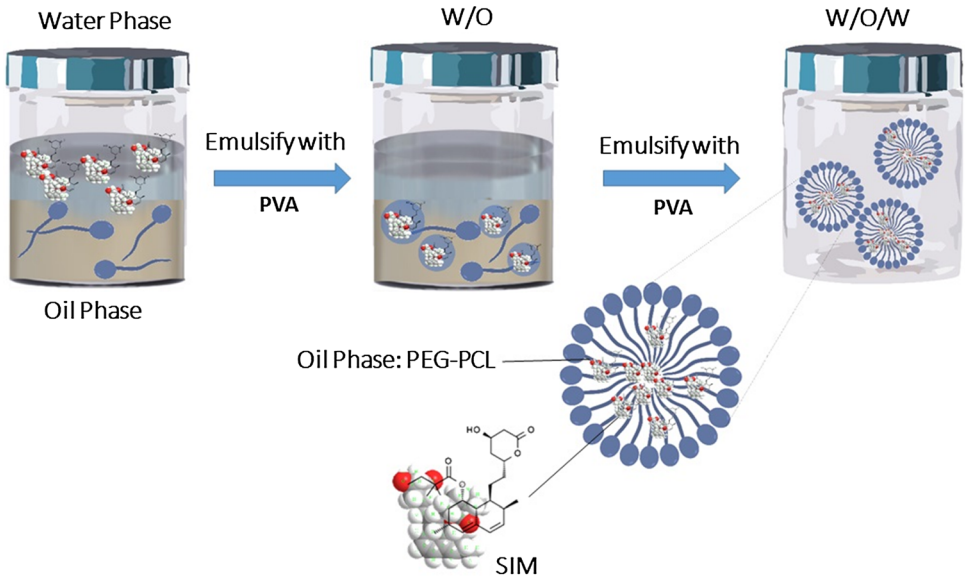

Fig. 1 Schematic representation of SIM loading process on the PCL-PEG NPs

% of poly (vinyl alcohol) under certain mixing rates (1500 rpm). Then, the mixture stirring was continued magnetically at room temperature until complete evaporation of the organic solvent. Subsequently, evaporation of the organic solvent in aqueous environment leads the amphiphilic copolymers to self-associate and form the nanoparticles. Finally, all of the samples were centrifuged at 20,000 × g, and freeze-dried (at pressure of 14 Pa and -78 0C) to remove all of the residual solvents and to produce the final nanoparticle form (Fig. 1).

Drug Encapsulation Efficiency and Drug Loading

To determine the efficiency of drug encapsulation, after the synthesis of drug-loaded NPs, the supernatant of the tube was isolated, and the quantity of non-entrapped SIM assessed was defined via Visible–UV spectrophotometer at 238 nm. In the following, the percent of (THE / AN) entrapped drug (Encapsulation Efficiency; EE) and drug loading (DL) were computed by employing the following formulas:

$$DL\ (\%) = \frac{Amount\ of\ drug\ entrapped}{Amount\ of\ NP} \times 100 \quad (1)$$

$$\mathrm{EE}\ (\%) = \frac{Amount\ of\ drug\ entrapped}{Amount\ of\ drug\ added} \times 100 \quad (2)$$

Characterization of NPs

The Dynamic Light Scattering (DLS) was utilized to analyze the NPs average size. The field emission scanning electron microscopy (FE-SEM) (MIRA3 TESCAN, Czech) was applied to determine NPs morphology. The structure confirmation of SIM-loaded NPs was investigated via Fourier transform infrared (FTIR) spectroscopy (BRUKER series). X-ray diffraction (XRD) measurements were achieved by a Bruker D8 Advance diffractometer using CuKα radiation (λ = 1.542 Å).

In Vitro Release Study

The 5 mg of SIM-encapsulated NPs were scattered in 30 ml phosphate-buffered solution (PBS) (pH = 5.5 and 7.4) and incubated with stirring at 37 °C. In various time periods, 3 ml PBS removed and the concentration of the released simvastatin measured using ultraviolet spectrofluorometric at the maximum absorption wavelength (238 nm). Then, buffer solution was substituted with the same volume of fresh PBS.

Cell Viability Assay

MCF-7 cells (human breast cancer cell line) were cultured in RPMI-1640 media containing 10% FBS (fetal bovine serum) and 1% streptomycin/penicillin and incubated at 5% humidity in sterile flasks. MTT (3-(4, 5-dimethylthiazole-2-yl)-2,5-biphenyl tetrazolium bromide) assay was utilized to study the viability of cells. Briefly, MCF-7 cells (5000 /well) were plated in 96-well plates and the day after treated with SIM, PCL-PEG, and SIM-loaded NPs (0–30 mM) for 48 h. Next, MTT solution (0.5 mg/mL, 200 µL) was added to all wells and incubated for 4 h. The 200 µL of DMSO was applied to solubilize the violet crystals. Plates were read using Beckmann Coulter ELISA plate reader (BioTek) at 570 nm at the final step.

DAPI Staining

The morphological features of apoptotic cells were assessed by DAPI nuclear staining. Firstly, MCF-7 cells (2×10^5 /well) were plated into 6–well plate and treated with SIM and SIM-loaded PCL-PEG NPs for 48 h. The cells were then fixed for 30 min with 4% ethanol, washed with PBS twice, and incubated for 30 min with 1 mg/mL DAPI at 37 °C. An inverted fluorescence microscope observed the stained cells.

The Analysis of Cell Cycle

The cell cycle phase of MCF-7 cells was characterized through flow cytometry. MCF-7 cells (2×10^5/mL density) were harvested 48 h after the treatment with SIM and SIM-loaded PCL-PEG NPs at different concentrations. Subsequently, cells were washed with PBS twice and fixed in 4 °C with ice-cold 70% ethanol for 24 h. Then, the fixed cells were collected and stained according to the RNAse/propidium iodide protocol. The cell cycle analysis was performed through a FACS Calibur cytometer.

Flow Cytometry Analysis

Apoptosis assay was performed utilizing an Annexin V Apoptosis Detection Kit (BD Bioscience). Briefly, MCF-7 cells (2×10^5) seeded in six-well plates were treated with SIM and SIM-loaded PCL-PEG NPs. Forty-eight hours followed by treatment, the cells were washed with PBS and harvested. Next, cells were suspended in a binding buffer containing PI (5 μL) and Annexin V (5 μL), and the mixture was incubated at room temperature in the dark for 15 min. Apoptotic cells were analyzed using flow cytometry.

RNA Isolation and Real-Time PCR Analysis

MCF-7 cells were plated into a 6-well plate and treated with SIM and SIM-loaded PCL-PEG NPs for 48 h, and then total RNA was extracted utilizing Trizol. Next, RNA quality and quantity were measured. Total RNA was changed to cDNA by Revert Aid First-strand cDNA synthesis Kit (Fermentas, Germany). Real time PCR amplification was conducted with a fluorescence thermal cycler system using SYBR Green master mix kit (Ampliqon; Odense, Denmark) with specific primers (Takapou Zist Co., Iran) (Table 1). The program of the real-time PCR was as follows; Initial denaturation in 95 °C for 5 min, 40 cycles of 95 °C for 15 s, and 60 °C for 30 s. Relative expression of each gene was normalized via housekeeping gene (GAPDH) and quantified utilizing the $2^{-\Delta\Delta Ct}$ method.

Statistical Analysis

Graph Pad Prism statistical software (USA, v.6.01) was utilized for analysis. Data are reported as the means ± standard deviation. The statistical significance was evaluated using one-way and two-way analyses of variances. $p < 0.05$ were considered as significant.

Results and Discussion

Synthesis of PCL-PEG Copolymer and FTIR Spectroscopy

In recent decades, there has been increasing interest in the preparation of drug-loaded polymers for a diversity of drug delivery purposes. However, until the last few years, there were very few published reports describing drug-conjugated nanoparticles [23, 24]. To the best of.

our knowledge, no study has yet been carried out on the conjugation of SIM with biodegradable polymers such as PCL-PEG for treatment of breast cancer cell line which can be used as the best drug carrier because some unique characteristics including improving the bioavailability as well as inducing passive targeting capability in the in-vivo.

PCL-PEG-PCL copolymer was synthesized successfully by ring-opening copolymerization of PEG and ε-caprolactone. FT-IR of SIM, PCL-PEG copolymers, and SIM-loaded PCL-PEG NPs is displayed in Fig. 2. The strong bands at 1727 and 1103 cm^{-1} are assigned to the presence of ether (C–O) and ester-carbonyl (C = O) groups. In FTIR spectra of SIM an obvious absorption is observed at 3553 cm^{-1} that is related to free O–H stretching, bands at 3015, 2964, 2882 cm^{-1} are associated with C–H stretching, and a sharp peak at 1722 cm^{-1} represents stretching vibration of the lactone carbonyl group and ester. These bands are distinct in the SIM-loaded PCL-PEG-PCL copolymer; also, no main shifting indicated the successful incorporation of SIM.

The Analysis of Morphology and Particle Size

Results of DLS showed that PCL/PEG NPs have uniform dispersion with an average size of 210 nm, zeta potential (ZP) of 26.5 ± 5.4 mV, and a polydispersity index (PDI) of 0.145 ± 0.054. Moreover, it is found that SIM-loaded PCL-PEG NPs showed an average size of 250 nm, ZP of 24.9 ± 4.5 mV, and PI of 0.105 ± 0.100 (Table 2). The obtained SEM images show that PCL/PEG NPs and PCL/PEG NPs loaded with SIM had spherical and uniform shapes (Fig. 3). According to the images, the average diameter of PCL/PEG NPs loaded with SIM was found to

Table 1 Primer sequences used in real-time PCR technique

Genes	Primer Sequence	PCR product size (bp)
Bax	F: 5′-GGTTGTCGCCCTTTTCTA-3′	108
	R: 5′- CGGAGGAAGTCCAATGTC -3′	
bcl-2	F: 5′- GATGTGATGCCTCTGCGAAG -3′	93
	R: 5′-CATGCTGATGTCTCTGGAATCT-3′	
P 53	F: 5′- AGA GTC TAT 5 V-GCT CGA CGC TAG-3′	125
	R: 5′-GAT CTG AC-3 V AGG CCC ACC CC-3′	
Cyclin D 1	F: 5′-AGACCTTCGTTGCCCTCTGT-3′	181
	R: 5′-CAGTCCGGGTCACACTTGAT-3′	
pRb	F: 5′-GCA TCG TCT GTA GTC TCG CCA ATA C-3′	176
	R: 5′-GCT CTG GGA TTT CTG CTT CTT CG-3′	
Fas	F: 5′-TGAAGGACATGGCTTAGAAGTG -3′	102

Table 2 Particle diameter, Polydispersity and zeta potential of drug loaded PLGA-PEG NPs

Formulation	Particle size (nm)[a]	Polydispersity index[a]	Zeta potential (mV)[a]
PCL/PEG NPs	210 ± 1.13	0.145 ± 0.054	26.5 ± 5.4
SIM-loaded PCL/PEG NPs	250 ± 5.26	0.105 ± 0.100	24.9 ± 4.5

[a]mean ± SD (n = 3)

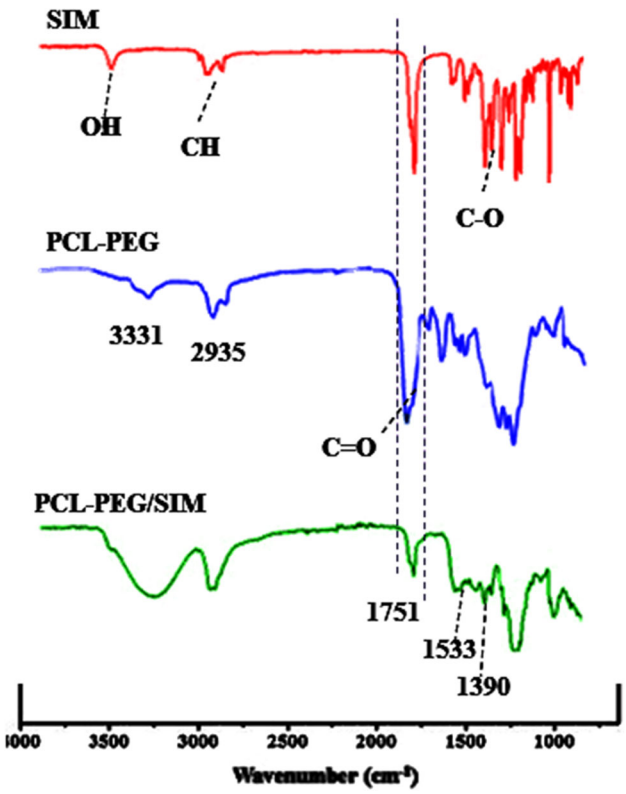

Fig. 2 FTIR spectra of SIM, PCL-PEG, and SIM-loaded PCL-PEG NPs

be approximately 250 nm. Considering the particle size analysis, SIM-loaded PCL-PEG NPs had larger diameters than blank PCL-PEG NPs, demonstrating that loading of SIM significantly enhanced NPs diameter distribution. The moderate deviation in diameter estimated through SEM and DLS is related to differences in the samples' surface characteristics under the employed assay settings. For example, NPs must be very dehydrated for analysis of SEM, while they are entirely hydrated when examined by DLS. The small size of NPs is necessary to escape from tracing and removal through the reticuloendothelial system.

Moreover, it is suggested which almost all cells preferentially internalize slightly positively charged NPs with a size less than 400 nm [25]. Hence, it can be said which the size range of SIM-loaded PCL-PEG NPs will be satisfactory to obtain a long half-life time when systemic circulation and also to target cancerous cells passively. The NPs surface charge is one of the main factors that affected the stability of NPs emulsion and their interaction with the cell membranes [26]. Moreover, the PCL–PEG–PCL NPs loaded with SIM can enhance the circulation time of drugs due to the negative charge of − 5.58 mV on their surface. Surface charge is also critical to determine whether NPs will assemble in the bloodstream or interact with or bind to the cell membrane with opposite charge [27]. The blood cells and plasma contain a negative charge, and NPs with a little negative charge on their surface may reduce non-specific interactions with these elements by electrostatic interactions [28].

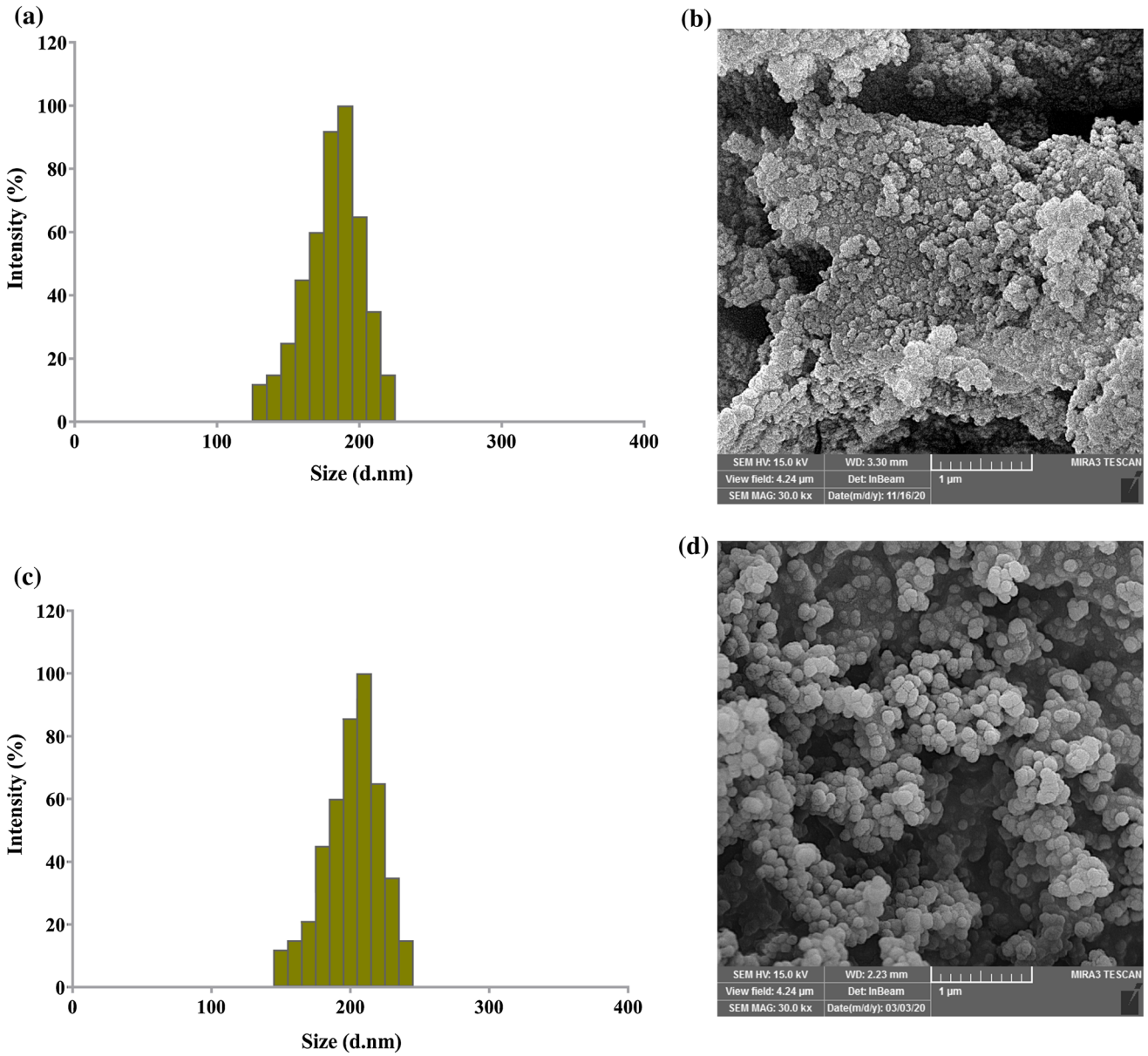

Fig. 3 Size distribution (**a**, **c**) and SEM images (**b**, **d**) where (**a**, **b**) PCL-PEG NPs; (**c**, **d**) SIM-loaded PCL-PEG NPs. The microspheres are uniform

Drug Loading and Entrapment Efficiency

The drug encapsulation efficiencies (EE) range was about 75.8 with a loading capacity of 11.4 ± 1.3%, respectively. The hydrophobic nature of SIM resulted in the high encapsulation efficiency of these anti-cancer agents.

X-ray Diffraction Patterns

XRD is frequently used to analyze the degree of sample crystallinity. The X-ray diffraction patterns of DHART solid dispersions are presented in Fig. 4. This crystalline Free DHART were characterized pattern with peaks at about 7.72, 10.61, 16.47, 17.12, 18.0, 21.28, 22.22, 26.0, 28.24, and 31.91 (2Theta). However, there was no clear peak in the XRD pattern for the amorphous polymer. The XRD pattern of the physical mixtures indicated that the intensities of typical peaks for the intact drug were lowered due to a dilution effect without a qualitative disparity in drug diffractogram (Fig. 4).

In vitro Drug Release

To study the role of chemical and biochemical agents on the SIM release from NPs, a work was applied on the NPs loaded with SIM in neutral and acidified (pH = 5) PBS

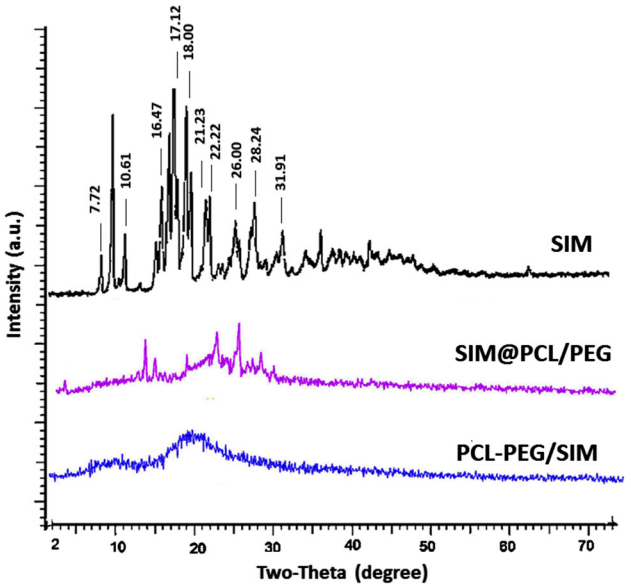

Fig. 4 Powder X-ray diffraction of SIM, SIM@PCL/PEG physical mixture, and PCL-PEG/SIM NPs

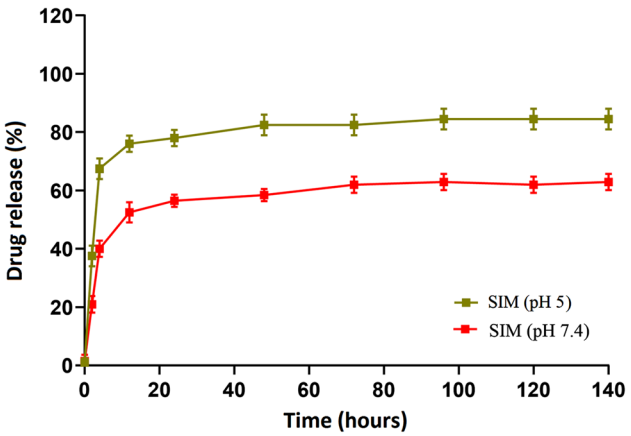

Fig. 5 Effect of different pH on drug release at 37 °C. Cumulative drug release patterns of SIM from PCL-PEG NPs at pH 5 and 7.4 (mean ± S.D., n = 3)

solution. Figure 5 shows the result of release patterns. As presented in Fig. 3, both PHs show an initial burst discharge during the first 4 h of incubation. Generally, the initial fast release phase is attributed to the molecules of the adsorbed drug on the NPs surface. According to Fig. 5, the release of SIM from the NPs was raised by reducing pH from 7.4 to 5. The released SIM in pH = 5 was significantly faster compared to in pH = 7.4 in simulated acidic situations of lysosomal/endosomal compartments (the SIM had a rapid release rate at pH 5 (mimicked acidic situations of lysosomal/endosomal compartments) compared to pH 7.4). For instance, 83.56% of the total SIM amount was released from NPs in pH 5 after the incubation 96 h, while the percentage of SIM released at pH = 7.4 was 62.99. Figure 5 also indicated that the maximum SIM released from the NPs after incubation for 120 h, in pH values of 5 and 7.4 is 84.45% and 63.41%, respectively. The sustained release of SIM probably is attributed to its encapsulation in the NPs inner part. Hence, copolymeric NPs can be significantly considered selective and sensitive nano-systems to deliver hydrophobic drugs for various therapeutic purposes.

In Vitro Cytotoxicity

As is clear from Fig. 6, MTT assay results indicated that the viability of the MCF-7 cells was remarkably decreased after treatment with SIM-loaded PCL-PEG NPs in dose-dependently than to free SIM in all concentrations. After incubation for 48 h, the IC_{50} values of free SIM were obtained as 1.97 mM and for SIM-NPs as and 3.3 mM, respectively. The IC_{50} values certainly revealed the excellent performance of SIM-NPs. The elevated cytotoxicity of PCL-PEG NPs loaded with SIM against MCF-7 cells was because of the great intracellular concentrations of SIM and its controlled release. It is proved that nano-systems internalize the encapsulated drugs by using a specific cellular pathway and release them as controlled, while free drugs can easily diffuse by the cell membrane [29]. So far, several studies were done to nanocapsule the SIM to apply it in hyperlipidemia treatment [30, 31]. However, applying polymeric NPs to deliver the SIM into cancer cells hasn't still been widely studied. Wu and coworkers assessed the efficiency of cholic Acid-Core Star-Shaped PLGA NPs to deliver the SIM into breast cancer cells (MDA-MB-231). The cytotoxicity assay data showed that star-shaped CA-PLGA loaded with SIM has a higher cytotoxicity effect than free SIM. Furthermore, results of in vivo study performed in the MDA-MB-231 xenograft tumor model indicated that star-shaped CA-PLGA loaded with SIM could efficiently repress the tumor growth in a greater period compared to free SIM [32].

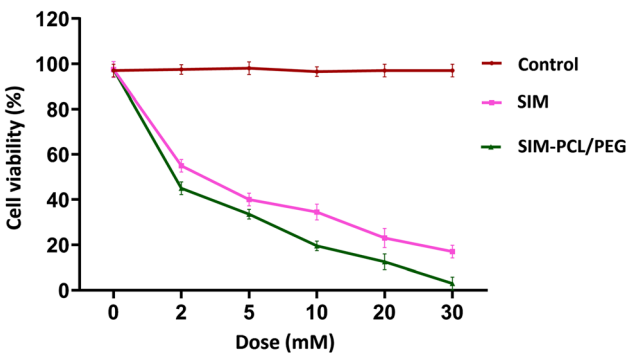

Fig. 6 In vitro cytotoxicity of SIM, and SIM-loaded PCL-PEG NPs over a range of concentrations (0–30 mM) in MCF-7 cells for 48 h of incubation (mean ± S.D., n = 3)

Detection of Chromosome Condensation using DAPI Staining

Changes in nuclear morphology of apoptotic cells were observed following DAPI staining after treatment with free SIM, and PCL-PEG NPs loaded with SIM (Fig. 7). After DAPI staining, the nucleus of untreated MCF-7 cells revealed homogeneous fluorescence color without any segmentation and fragmentation. Treating the cells with free SIM and PCL/PEG NPs loaded with SIM resulted in the nuclei segregation into fragments, confirming the breakdown in chromatin followed via condensation of DNA. According to Fig. 7, the percentage of apoptotic cells treated with PCL/PEG NPs loaded with SIM was remarkably greater compared to free SIM, indicating that SIM loaded on PCL/PEG NPs induced apoptosis in MCF-7 cells more efficiently than free SIM.

Cell Cycle Arrest Analysis

In Fig. 8, the effects of free SIM and PCL/PEG NPs loaded with SIM against cell-cycle progress in MCF-7 cells. The fundamental increase in the population of the MCF-7 cells in the sub-G1 phase was observed followed by treating with PCL/PEG NPs loaded with SIM than free SIM. As is clear from Fig. 8, the treated MCF-7 cells with NPs loaded with SIM for 48 h indicated a noticeable increase in the sub-G1 population (70.23%) than free SIM (51.3%) ($p < 0.05$). The S and G2 phases' population decreased after an upsurge in the sub-G1 phase compared to free SIM. The damage of DNA was proposed as a major reason for the arrest of the cell cycle. The cells containing damaged DNA tend to accumulate in the G1 or the G2/M phases, whereas cells with irreversible damage are collected in the sub-G1 phase [33]. The data obtained from the present study showed that the effects of free SIM and loaded on PCL-PEG NPs on apoptosis activation are associated with changes in cell cycle progress via the increase in cells entering the sub-G1 phase.

PI/Annexin V Staining

To quantify the proportion of dead and apoptotic MCF-7 cells following treatment with SIM and SIM-loaded PCL-PEG NPs, PI/Annexin V staining was utilized (Fig. 9). Data showed that SIM results in the induction of cell death in MCF-7 cells. The free SIM and loaded on NPs enhanced the percentage of dead MCF-7 cells to 21.26 and 29.63%, respectively than control. These results showed that cell cycle progress and apoptosis probably are linked with elevated endocytosis and release kinetics of encapsulated SIM. There is increasing evidence that SIM could increase apoptosis or reduce the proliferation of various cancer cells like prostate cancer, medulloblastoma brain tumor, lung,

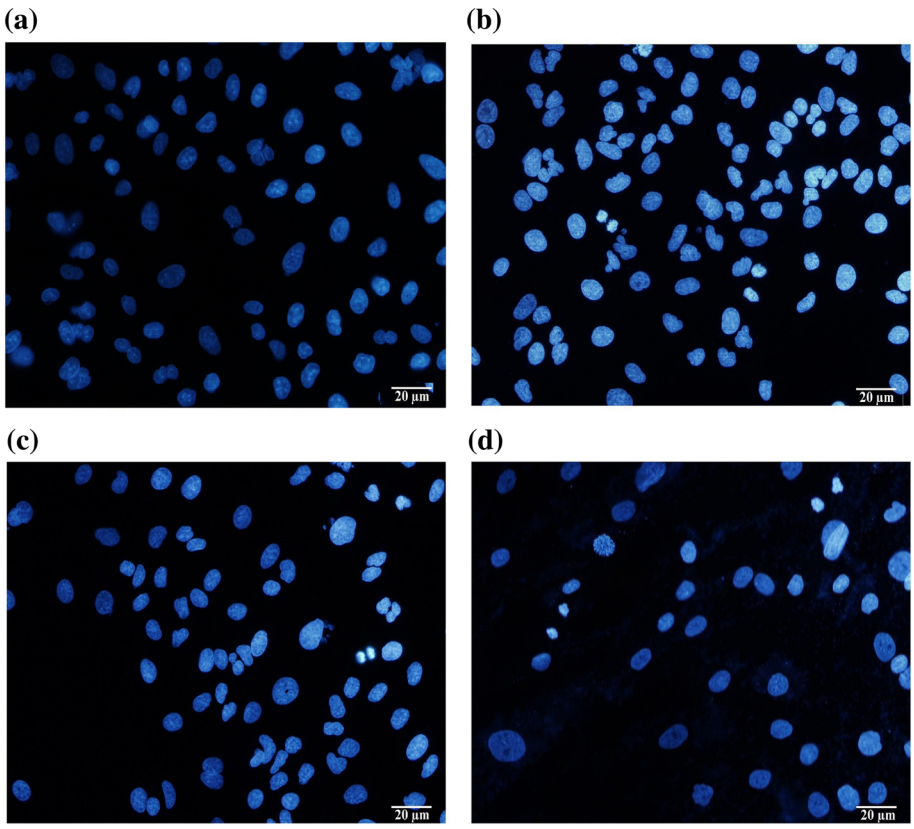

Fig. 7 Morphological changes in the cells treated with free SIM and SIM-loaded PCL-PEG NPs that are detected using fluorescence microscopy

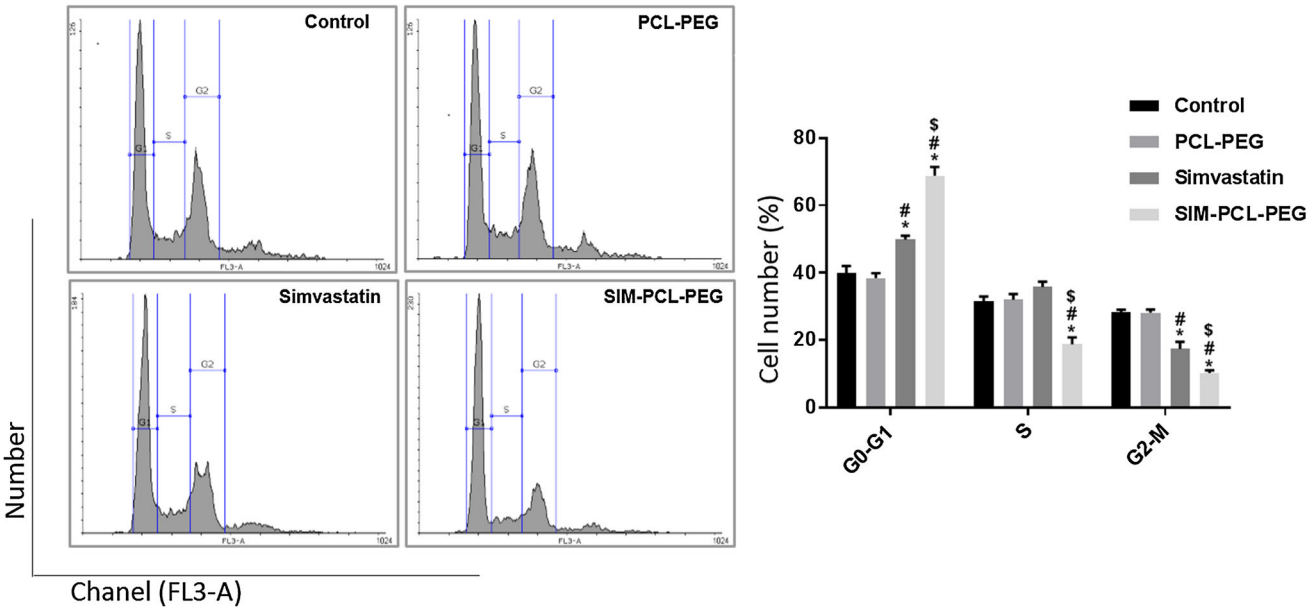

Fig. 8 Cell cycle analysis of control cells and MCF-7 cells exposed with IC50 concentration of free SIM and SIM-loaded PCL-PEG NPs for 48 h

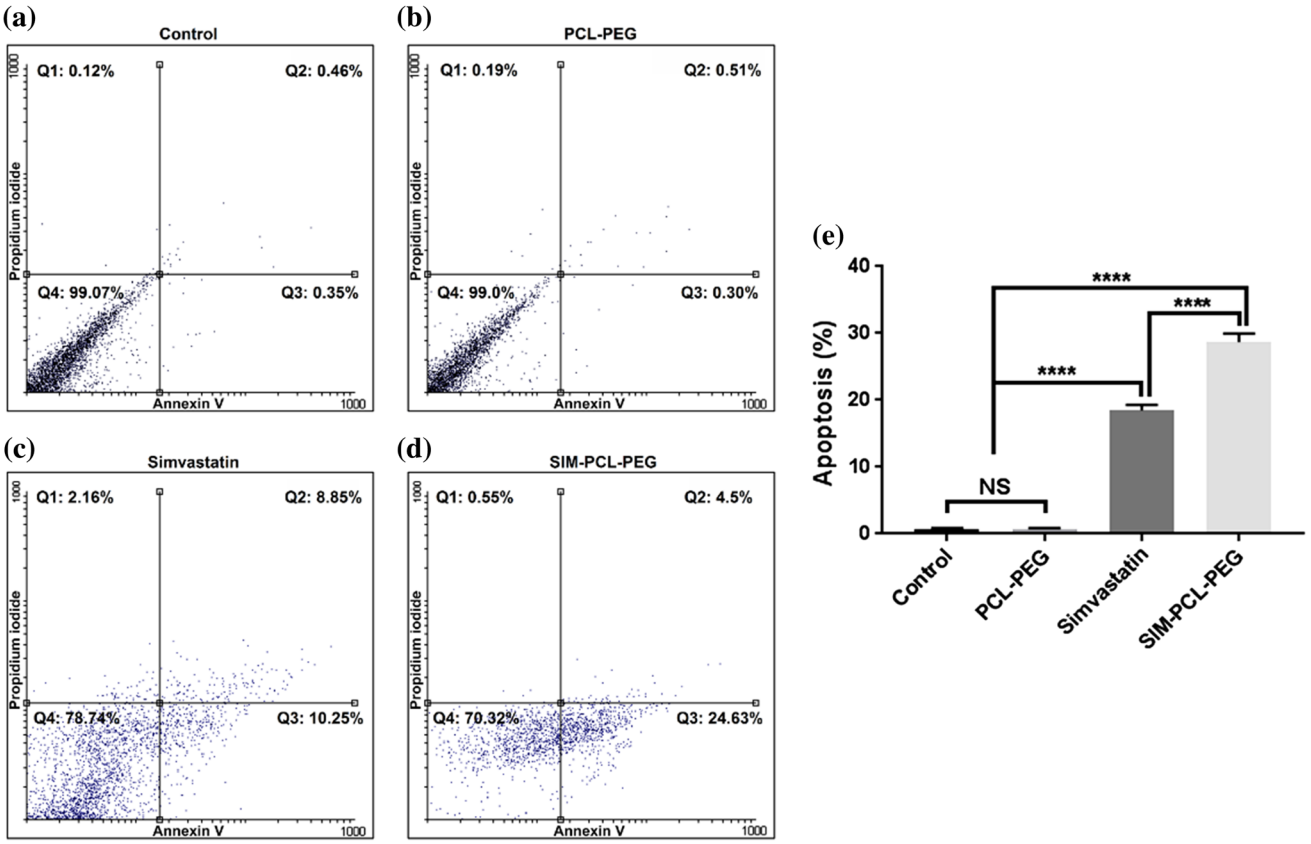

Fig. 9 The induction of apoptosis in treated MCF-7 cells with IC50 concentrations of free SIM and SIM-loaded PCL-PEG NPs for 48 h

and cancer stem cells [5, 11]. In conformance to prior reports, our study showed that free SIM and SIM-loaded PCL-PEG NPs significantly suppressed breast cancer cells proliferation. It has been suggested that SIM induced arrest of the cell cycle via suppressing the STAT3/SKP2 axis and activating the AMPK to promote the accumulation of p21

and p27 in hepatocellular carcinoma cells [34]. Furthermore, a recent study on nasopharyngeal carcinoma showed that treatment with SIM induced arrest of C666-1 cells in the G1 phase by repressing the expression of cyclin D1 and Cdk4 and improving the expression of p27 [35].

The Analysis of Gene Expression

To recognize the molecular mechanisms behind the antiproliferative properties of SIM-loaded NPs in MCF-7 cells, the expression of genes involved in the apoptosis pathway (Bcl-2, Bax, Fas) and cell cycle regulating genes (p53, cyclin D, and pRb) were measured (Fig. 10). The real-time PCR data exhibited that the expression level of apoptotic genes Bax and Fas, also cell cycle-regulating genes p53, was remarkably more up-regulated in treated MCF-7 cells with SIM-loaded NPs than treated cells with treated cells free SIM. Moreover, the mRNA expression level of Bcl-2, cyclin D, and pRb genes was significantly more down-regulated in SIM-NPs treated cells compared to treated cells with free SIM. Apoptosis plays an important role in cancer pathogenesis; therefore (THE / A) study of genes involved in this pathway is important in research on the initiation and progression of cancer.

Bcl-2 is an anti-apoptotic protein, while Bax protein promotes cell death. The formation of Bcl2–Bax heterodimer provokes a signal for the survival of cells. These proteins are transcriptional targets for p53, which cause the induction of apoptosis in response to DNA damage [36]. Previous studies have shown that the Bcl-2/Bax ratio can influence the progression of the tumor and its aggressiveness [37, 38].

The prenylation of Ras proteins is used for the growth, signaling, and cycle of cells by cancer cells with up-regulated metabolism [39]. The cell cycle genes play a crucial role in keeping genomic stability and employ genetic monitoring following exposure to damaging agents, including oxidative stress, chemicals, and UV and gamma radiation. Accordingly, to verify cells arrest in G0/G1 phase, the expression of TP53 gene, which induces cell cycle arrest or apoptosis, CDK1, which is known as responsible for the progress of cell cycle, and CDKN1A (the cyclin-dependent kinase inhibitor), which acts as a regulator of the cell cycle progression in G1, were evaluated [39].

Our study assessed the induction level of apoptosis in treated MCF-7 cells with free SIM and PCL/PEG NPs loaded with SIM, and the results were proved prior studies. Koyuturk et al. indicated that SIM induces apoptosis by the JNK involvement in breast cancerous cells independent of the situation of their p53 expression [40]. In MCF-7 cells, SIM increased the fragmentation of DNA and at the molecular level induced the Bax overexpression, a pro-apoptotic gene, as well as the Bcl-2 suppression, the gene that protects cells from apoptosis [41]. Moreover, investigations by Sheikholeslami et al. indicated that apoptosis in medulloblastoma brain tumor cell lines is controlled by prenylation intermediates of the cholesterol metabolism pathway. Also, they were demonstrated that SIM induces the activity of caspases such as caspase 3, 7, 8, and 9, and changes the expression of regulator proteins associated with apoptosis, including Bcl-xl, Bcl-2, and Bax [5]. Consistent with our work, Karlic and colleagues reported the influence of SIM on the proliferation and signaling of cells in U-2 OS and MG-63 osteosarcoma cells, MDA-MB-231 breast cancer, and PC-3 prostate carcinoma. Results showed that SIM induced the cell cycle arrest in G1 in U-2 OS, MDA-MB-23, and PC-3 cells, while the arrest of the cell cycle was more found in S-phase in MG-63 cells [42].

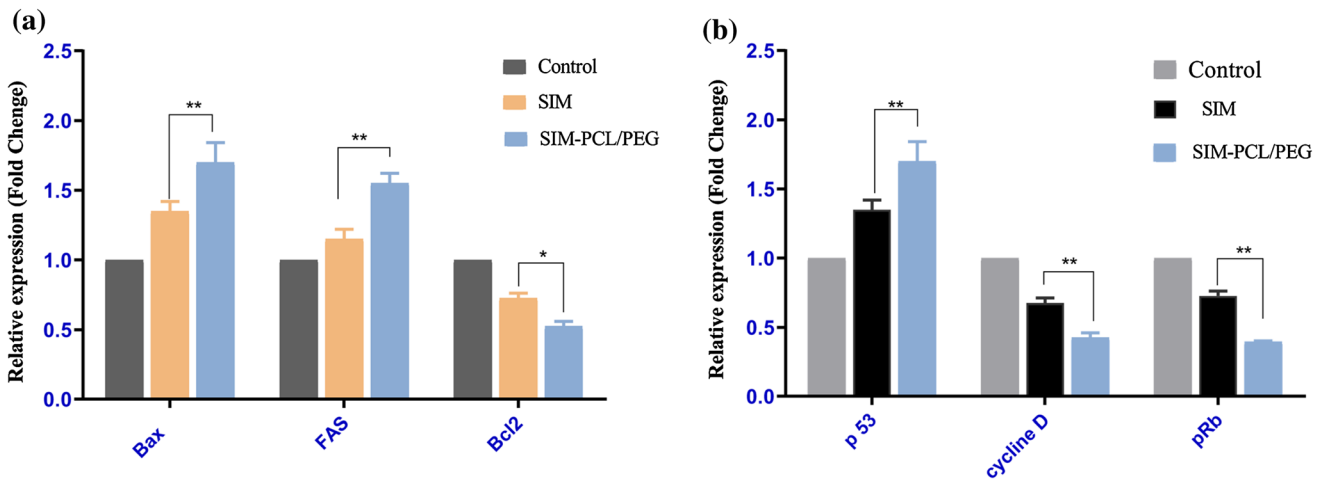

Fig. 10 The expression levels of Bax, FAS, Bcl-2 (**a**), p53, Cyclin D1, and pRb genes (**b**), relative to reference gene (GAPDH) in MCF-7 cells treated with free SIM and SIM-loaded PLC-PEG NPs

Conclusion

In this study, NPs prepared by a double emulsion method from copolymer PCL/PEG were used as carriers to deliver SIM into MCF-7 cells for breast cancer chemotherapy. Based on our results, PCL/PEG NPs loaded with SIM could kill breast cancer cells more quickly than free SIM, so potentially this strategy can reduce cytotoxicity and patient side effects. Moreover, according to our results, nano-formulation of SIM with PCL-PEG can suppress Bcl-2, cyclin D, and pRb genes and induce apoptosis of human breast cancerous MCF-7 cells more than free SIM; hence this nanostructure of SIM has significant potential to use as a complement drug for the treatment of breast cancer. These results indicate that the loading of SIM in PCL-PEG NPs as we have shown here, could lead to promising candidates for breast cancer treatment with a specific final goal of reducing drug resistance related to the current clinically used therapeutics.

Acknowledgements The authors express their sincere thanks to the pharmaceutical sciences research center of Ardabil University of Medical Sciences for financial support.

Authors' Contribution The conception and the design of the study were performed by KN. The experiments were carried out by all authors. Data collection and analyses were conducted by MG and MD. The project was supervised by KN. The manuscript was drafted by MD, and revised by KN. All authors participated in the manuscript in the critical review process of the manuscript and approval of the final version.

Declarations

Conflict of interest The authors declare no conflict of interest.

References

1. K. Nurgali, R. T. Jagoe, and R. Abalo (2018). Adverse effects of cancer chemotherapy: anything new to improve tolerance and reduce sequelae? *Fronti. Pharmacol.* **9**, 245.
2. Y. Tang, et al. (2016). Classification, treatment strategy, and associated drug resistance in breast cancer. *Clinical Breast Cancer* **16** (5), 335–343.
3. E. Miller, et al. (2014). Current treatment of early breast cancer: adjuvant and neoadjuvant therapy. *F1000Research* **3**, 198.
4. G. Fritz, et al. (2002). Rho GTPases in human breast tumours: expression and mutation analyses and correlation with clinical parameters. *Br. J. Cancer* **87** (6), 635–644.
5. K. Sheikholeslami, et al. (2019). Simvastatin induces apoptosis in medulloblastoma brain tumor cells via mevalonate cascade prenylation substrates. *Cancers* **11** (7), 994.
6. K. Nejati-Koshki, A. Akbarzadeh, and M. Pourhassan-Moghaddam (2014). Curcumin inhibits leptin gene expression and secretion in breast cancer cells by estrogen receptors. *Cancer Cell Internat.* **14** (1), 1–7.
7. S. Samadzadeh, et al. (2021). In vitro anticancer efficacy of Metformin-loaded PLGA nanofibers towards the post-surgical therapy of lung cancer. *J. Drug Delivery Sci. Technol.* **61**, 102318.
8. P. M. Tricarico, S. Crovella, and F. Celsi (2015). Mevalonate pathway blockade, mitochondrial dysfunction and autophagy: a possible link. *Int. J. Mol. Sci.* **16** (7), 16067–16084.
9. M. Thurnher, G. Gruenbacher, and O. Nussbaumer (2013). Regulation of mevalonate metabolism in cancer and immune cells. *Biochimica et Biophysica Acta (BBA) Molecular and Cell Biology of Lipids* **1831** (6), 1009–1015.
10. J. Clendening and L. Penn (2012). Targeting tumor cell metabolism with statins. *Oncogene* **31** (48), 4967–4978.
11. E. Arabizadeh, et al. (2019). Potential effect of simvastatin as an anti-cancer agent on SOX7 and SOX9 expression in prostate cancer cell lines. *Shiraz E-Med J.* https://doi.org/10.5812/semj.69057.
12. A. El-Sohemy and M. C. Archer (2000). Inhibition of N-methyl-N-nitrosourea-and 7, 12-dimethylbenz [a] anthracene-induced rat mammary tumorigenesis by dietary cholesterol is independent of Ha-Ras mutations. *Carcinogenesis* **21** (4), 827–831.
13. G. P. Nagaraju, et al. (2012). The impact of curcumin on breast cancer. *Integrative Biol.* **4** (9), 996–1007.
14. A. Firouzi-Amandi, et al. (2018). Chrysin-nanoencapsulated PLGA-PEG for macrophage repolarization: Possible application in tissue regeneration. *Biomed. Pharmacotherapy* **105**, 773–780.
15. R. Zamani, et al. (2018). Recent advances in cell electrospining of natural and synthetic nanofibers for regenerative medicine. *Drug Res.* **68** (08), 425–435.
16. M. Dadashpour, et al. (2018). Watercress-based electrospun nanofibrous scaffolds enhance proliferation and stemness preservation of human adipose-derived stem cells. *Artificial Cells, Nanomed. Biotechnol.* **46** (4), 819–830.
17. K. Nejati, et al. (2021). Biomedical applications of functionalized gold nanoparticles: a review. *J Cluster Sci*. https://doi.org/10.1007/s10876-020-01955-9.
18. Y. Panahi, et al. (2017). Preparation, surface properties, and therapeutic applications of gold nanoparticles in biomedicine. *Drug Res.* **11** (02), 77–87.
19. M. Zamani, et al. (2018). In vitro and in vivo biocompatibility study of folate-lysine-PEG-PCL as nanocarrier for targeted breast cancer drug delivery. *European Polymer J.* **103**, 260–270.
20. H. Nosrati, et al. (2019). Biotin-functionalized copolymeric PEG-PCL micelles for in vivo tumour-targeted delivery of artemisinin. *Artificial Cells, Nanomed. Biotechnol.* **47** (1), 104–114.
21. R. M. Dhahi, et al. (2016). Therapeutic targeting of anti-cancer drug Loaded PCL-PEG-PCL triblock copolymer nanoparticles toward MCF-7 breast cancer cell line. *Int. J. Scientific Eng. Res.* **7** (5), 1238–1244.
22. C. Hu, et al. (2017). Micelle or polymersome formation by PCL-PEG-PCL copolymers as drug delivery systems. *Chinese Chem. Lett.* **28** (9), 1905–1909.
23. K. Rostamizadeh, et al. (2018). Methotrexate-conjugated mPEG–PCL copolymers: a novel approach for dual triggered drug delivery. *New J. Chem.* **42** (8), 5937–5945.
24. H. R. K. Manjili, et al. (2016). Preparation and physicochemical characterization of biodegradable mPEG-PCL core-shell micelles for delivery of artemisinin. *Pharm. Sci.* **22** (4), 234–243.
25. B. Xiao, et al. (2015). Co-delivery of camptothecin and curcumin by cationic polymeric nanoparticles for synergistic colon cancer combination chemotherapy. *J. Mater. Chem. B* **3** (39), 7724–7733.
26. E. Fröhlich (2012). The role of surface charge in cellular uptake and cytotoxicity of medical nanoparticles. *Int. J. Nanomed.* **7**, 5577.
27. A. Kumari, S. K. Yadav, and S. C. Yadav (2010). Biodegradable polymeric nanoparticles based drug delivery systems. *Colloids and surfaces B: Biointerfaces* **75** (1), 1–18.

28. M. Turner, G. Clough, and C. Michel (1983). The effects of cationised ferritin and native ferritin upon the filtration coefficient of single frog capillaries Evidence that proteins in the endothelial cell coat influence permeability. *Microvascular Res* **25** (2), 205–222.
29. K. Murugan, et al. (2015). Parameters and characteristics governing cellular internalization and trans-barrier trafficking of nanostructures. *Int. J. Nanomed.* **10**, 2191.
30. S. Z. H. Rizvi, et al. (2019). Simvastatin-loaded solid lipid nanoparticles for enhanced anti-hyperlipidemic activity in hyperlipidemia animal model. *Int. J. Pharm.* **560**, 136–143.
31. G. I. Harisa, A. H. Alomrani, and M. M. Badran (2017). Simvastatin-loaded nanostructured lipid carriers attenuate the atherogenic risk of erythrocytes in hyperlipidemic rats. *Eu. J. Pharm. Sci.* **96**, 62–71.
32. Y. Wu, et al. (2015). Novel simvastatin-loaded nanoparticles based on cholic acid-core star-shaped PLGA for breast cancer treatment. *J Biomed. Nanotechnol* **11** (7), 1247–1260.
33. W. Chunyan and S. Valiyaveettil (2013). Correlation of biocapping agents with cytotoxic effects of silver nanoparticles on human tumor cells. *RSC Adv.* **3** (34), 14329–14338.
34. S.-T. Wang, et al. (2017). Simvastatin-induced cell cycle arrest through inhibition of STAT3/SKP2 axis and activation of AMPK to promote p27 and p21 accumulation in hepatocellular carcinoma cells. *Cell Death Dis.* **8** (2), e2626–e2626.
35. Z. Ma, et al. (2019). Inhibitory effect of simvastatin in nasopharyngeal carcinoma cells. *Experimental Therapeutic Med.* **17** (6), 4477–4484.
36. S. Zohre, et al. (2014). Trichostatin A-induced apoptosis is mediated by Kruppel-like factor 4 in ovarian and lung cancer. *Asian Pacific J. Cancer Prevention* **15** (16), 6581–6586.
37. D. R. McIlwain, T. Berger, and T. W. Mak (2013). Caspase functions in cell death and disease. *Cold Spring Harbor Perspect. Biol.* **5** (4), a008656.
38. S. Amirsaadat, et al. (2021). Metformin and Silibinin co-loaded PLGA-PEG nanoparticles for effective combination therapy against human breast cancer cells. *J Drug Delivery Sci Technol* **61**, 102107.
39. S. Kany, et al. (2018). Simvastatin exerts anticancer effects in osteosarcoma cell lines via geranylgeranylation and c-Jun activation. *Int. J. Oncol* **52** (4), 1285–1294.
40. M. Koyuturk, M. Ersoz, and N. Altiok (2007). Simvastatin induces apoptosis in human breast cancer cells: p53 and estrogen receptor independent pathway requiring signalling through JNK. *Cancer Lett.* **250** (2), 220–228.
41. C. Spampanato, et al. (2012). Simvastatin inhibits cancer cell growth by inducing apoptosis correlated to activation of Bax and down-regulation of BCL-2 gene expression. *Int. J. Oncol.* **40** (4), 935–941.
42. H. Karlic, et al. (2017). Statin and bisphosphonate induce starvation in fast-growing cancer cell lines. *International journal of molecular sciences* **18** (9), 1982.